Scholars Journal of Engineering and Technology

OPEN ACCESS

Abbreviated Key Title: Sch J Eng Tech
ISSN 2347-9523 (Print) | ISSN 2321-435X (Online)
Journal homepage: https://saspublishers.com

Stability, Scalability, and Sustainability Challenges in Perovskite Solar Cells: A Multi-Scale Computational Investigation

Muhammad Shoaib[1]*, Muhammad Waqas[1], Aamir Ali[1], Yasoob Ali Khan[2], Moazzam Ali[2], Muhammad Yousof[2], Muhammad Adeel[2], Muhammad Noorulhassan[3]

[1]Material Science and Technology, National University of Science and technology MISIS
[2]University of Sargodha
[3]Thal University Bhakkar

DOI: https://doi.org/10.36347/sjet.2026.v14i09.004 | **Received:** 22.07.2026 | **Accepted:** 14.09.2026 | **Published:** 16.09.2026

***Corresponding author:** Muhammad Shoaib
Material Science and Technology, National University of Science and technology MISIS

Abstract | **Original Research Article**

Perovskite solar cells (PSCs) have demonstrated unprecedented efficiency gains, rising from under 4% to certified single-junction power conversion efficiencies (PCEs) exceeding 26%. However, their commercial deployment is strictly constrained by the "efficiency–stability–scalability–sustainability" quad lemma. In this computational research article, we implement a multi-scale modeling framework integrating Density Functional Theory (DFT), Ab Initio Molecular Dynamics (AIMD), Finite Element Method (FEM) drift-diffusion/fluid dynamics, and quantitative Life Cycle Assessment (LCA). DFT and AIMD calculations delineate the atomic-scale energetics of point defect formation, iodide vacancy (V_I) migration, and moisture-induced phase degradation across organometal ($MAPbI_3$, $FAPbI_3$) and inorganic ($CsPbI_3$) systems. FEM fluid-dynamics and drift-diffusion models capture the fluid instabilities, thickness non-uniformities, and non-radiative recombination hotspots that arise during large-area slot-die and blade coating. Finally, LCA simulations quantify energy payback times (EPBT) and USEtox ecotoxicity indices for lead-based versus lead-free (Sn/Bi) halide absorbers and green solvent systems.

Keywords: Perovskite solar cells, Commercialization quadlemma, Multi-scale modeling, Defect energetics, Ion migration, Composition engineering.

1. INTRODUCTION

Metal halide perovskites have emerged as one of the most intensively investigated classes of photovoltaic absorber materials because of their exceptional optoelectronic properties, compositional flexibility, and compatibility with low-temperature solution processing. These materials generally adopt the ABX_3 perovskite structure, where A represents a monovalent organic or inorganic cation, such as methylammonium ($MA^+ = CH_3NH_3^+$), formamidinium ($FA^+ = HC(NH_2)_2^+$), or cesium (Cs^+); B represents a divalent metal cation, most commonly Pb^{2+} or Sn^{2+}; and X represents a halide anion, typically I^-, Br^-, or Cl^-. The ability to independently modify the A-site, B-site, and halide sublattice provides an unusually broad compositional design space in which crystal structure, bandgap, defect chemistry, carrier transport, and environmental stability can be systematically tuned [1–3, 5].

The rapid development of perovskite photovoltaics has been driven by a combination of strong optical absorption, long charge-carrier diffusion lengths, favorable charge-transport characteristics, low exciton binding energies, and comparatively high tolerance toward certain intrinsic defects [2, 3, 5, 6]. Early demonstrations rapidly established the photovoltaic potential of organometal halide perovskites, while subsequent improvements in composition, interfaces, morphology, and device architecture resulted in a remarkable increase in power conversion efficiency (PCE). Perovskite solar cells (PSCs) have therefore progressed from an emerging laboratory technology toward a potentially disruptive photovoltaic platform capable of competing with established silicon photovoltaics [1, 2, 4].

Despite this extraordinary efficiency evolution, the transition from laboratory-scale devices to reliable commercial modules remains unresolved. In particular,

the record efficiency achieved on small-area cells does not automatically translate into equivalent performance over large areas or over prolonged operating periods. The fundamental difficulty arises because PSC performance is controlled simultaneously by processes occurring over widely separated spatial and temporal scales. Atomic-scale defects and lattice distortions influence ion migration and electronic recombination; these phenomena affect mesoscale film morphology and interfaces; coating and crystallization processes determine large-area thickness uniformity; and manufacturing choices ultimately influence energy consumption, emissions, toxicity, and end-of-life impacts. Consequently, efficiency, operational stability, manufacturing scalability, and environmental sustainability should not be considered as independent optimization targets. Instead, they form a coupled performance–stability–scalability–sustainability problem, referred to in this work as the PSC commercialization quadlemma [4, 9, 12, 18].

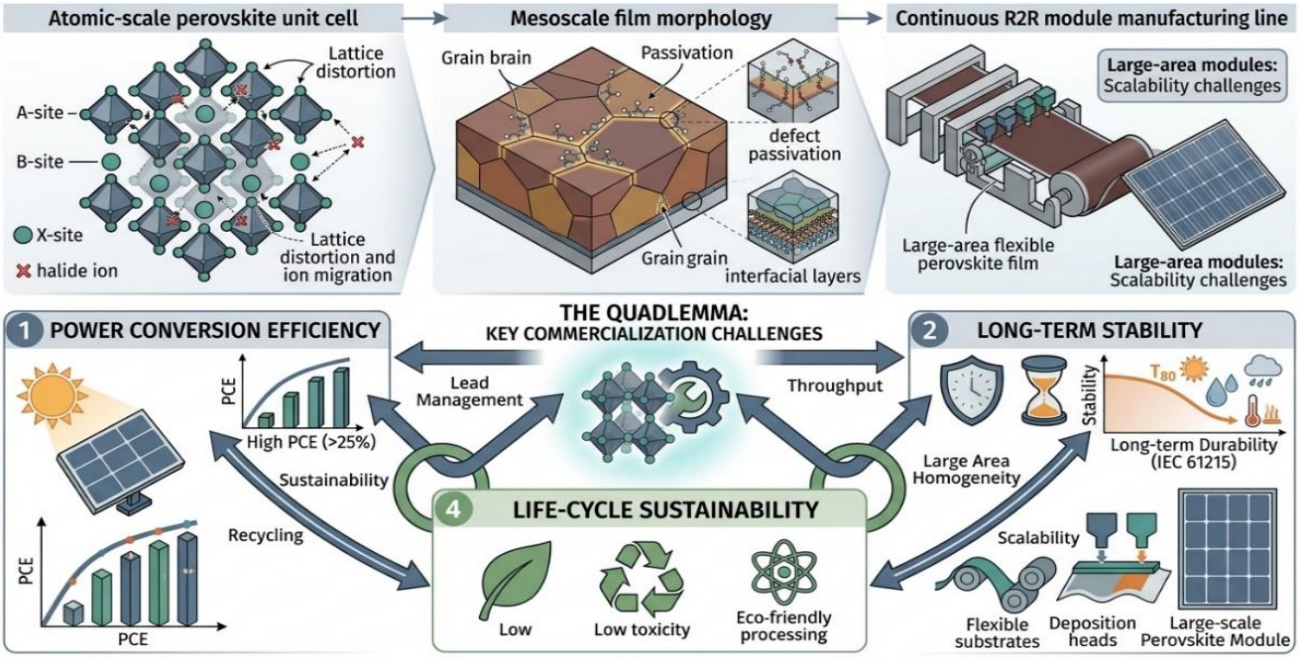

Figure 1

1 Exceptional Photophysical Properties and the Efficiency–Stability Trade-Off

The attractiveness of metal halide perovskites originates from their combination of strong light absorption and efficient charge generation and transport. Their absorption coefficients can exceed 10^5 cm^{-1}, enabling substantial photon absorption within relatively thin absorber layers. In addition, experimental investigations have demonstrated charge-carrier diffusion lengths exceeding 1 μm in high-quality perovskite films, highlighting the potential for efficient extraction of photogenerated carriers even in relatively thin devices [3]. The electronic structure can also be continuously modified through compositional substitution, particularly by changing the halide composition or A-site cation. This tunability enables the design of absorbers for different photovoltaic architectures and spectral requirements [2, 5, 17].

At the atomic level, the relatively soft ionic lattice provides both advantages and disadvantages. Lattice flexibility can accommodate compositional variations and contribute to defect tolerance, but it also permits significant structural fluctuations and dynamic disorder. The same structural characteristics that facilitate defect accommodation can therefore enable ionic motion under operating conditions. Computational investigations have shown that point defects, particularly halide vacancies, play an important role in determining the electronic and chemical behavior of perovskite absorbers [6, 13–15]. Consequently, the fundamental challenge is not simply to maximize the initial electronic quality of a perovskite absorber, but to engineer a material whose favorable optoelectronic properties remain stable under simultaneous illumination, electrical bias, elevated temperature, and environmental exposure.

This creates an intrinsic efficiency–stability trade-off. Compositions and processing conditions that produce high initial PCE may not necessarily provide the defect energetics, phase stability, and interfacial robustness required for long-term operation. A computational framework capable of connecting composition with defect formation energy, migration barriers, structural stability, and device-level consequences is therefore particularly valuable.

2 Intrinsic and Extrinsic Instability of Perovskite Absorbers

Operational instability remains one of the most important obstacles to the commercialization of PSCs. Perovskite degradation is governed by a combination of

intrinsic material processes and extrinsic environmental stresses. Important external stressors include moisture, oxygen, heat, illumination, electrical bias, and combinations of these factors [7, 8]. The degradation response is therefore highly dependent on the interaction between the perovskite lattice and its surrounding environment.

Moisture is particularly important because water can interact strongly with the ionic lattice and facilitate structural and chemical transformations. Water exposure can initiate hydration-related processes, modify local coordination environments, and promote the formation of degradation products. Thermal stress can further accelerate decomposition and chemical reactions, while photo-induced processes can promote changes in halide distribution and local composition [7, 8]. These degradation pathways are especially significant because practical photovoltaic modules operate under conditions in which temperature, illumination, humidity, and electrical stress vary continuously.

A second fundamental mechanism is ion migration. The relatively soft and dynamically disordered perovskite lattice permits mobile ionic defects to move under thermal gradients and electrical fields. Halide vacancies are particularly important because they can act as pathways for iodide or bromide migration. Experimental and theoretical studies have established that ionic motion can contribute to transient electrical behavior, hysteresis, degradation, and changes in local composition [13–15, 24–26].

Ion migration is not an isolated atomic-scale phenomenon. Redistribution of halide ions can create local variations in composition and electrostatic potential, alter interfacial charge distributions, generate defect-rich regions, and modify non-radiative recombination. Under illumination, mixed-halide materials can additionally undergo light-induced compositional redistribution and phase segregation. Such changes can reduce the effective electronic quality of the absorber and contribute to long-term performance loss.

The relationship between ion migration and device hysteresis is also particularly important. Mobile ions can accumulate near interfaces and modify internal electric fields, producing transient changes in current–voltage characteristics. Studies of rate-dependent J–V hysteresis and mobile-ion effects demonstrate that ionic and electronic processes are strongly coupled in operating PSCs [24–26]. Therefore, a realistic computational treatment of stability must extend beyond static crystal structures and incorporate defect energetics, finite-temperature lattice dynamics, and the interaction of mobile defects with device-scale electric fields.

3 Composition Engineering as a Route to Enhanced Stability

The large compositional design space of perovskites provides an opportunity to engineer stability through controlled substitution at the A-, B-, and X-sites. In particular, mixed-cation formulations containing FA^+ and Cs^+ have attracted considerable attention because they can improve structural stability, reproducibility, and photovoltaic performance compared with some single-cation compositions [16, 17].

The incorporation of multiple A-site cations modifies lattice dimensions, structural distortion, phase stability, and the local energetic landscape experienced by mobile defects. From a computational perspective, these effects can be quantified through lattice parameters, tolerance factors, defect formation energies, and migration barriers. Such quantities provide a direct connection between atomic structure and experimentally relevant stability.

For example, the present computational framework evaluates iodide-vacancy formation and migration behavior across representative $MAPbI_3$, $FAPbI_3$, $CsPbI_3$, and mixed-cation compositions. The resulting defect energetics provide a mechanistic basis for understanding why selected mixed-cation systems can suppress ionic transport. The objective is therefore not simply to identify a composition with a high theoretical PCE, but to identify compositions in which favorable electronic properties are accompanied by increased resistance to defect-mediated degradation.

4 Scale-Up from Laboratory Cells to Large-Area Modules

The second major commercialization barrier is the loss of performance during scale-up. Laboratory PSCs are commonly fabricated on small substrates using spin coating and highly controlled processing conditions. Under such conditions, precursor concentration, substrate temperature, solvent evaporation, nucleation, crystallization, and annealing can be carefully optimized. However, these conditions become substantially more difficult to maintain when the active area increases from fractions of a square centimeter to tens or hundreds of square centimeters [9, 10].

Large-area manufacturing requires deposition methods that are compatible with continuous or semi-continuous production. Technologies such as slot-die coating, blade coating, spray coating, and roll-to-roll processing provide promising pathways toward scalable manufacturing [10, 19–23]. Nevertheless, these techniques introduce additional fluid-dynamic and mass-transfer phenomena that are less significant in conventional small-area spin coating.

During solution deposition, the precursor ink forms a moving liquid film whose behavior depends on viscosity, surface tension, coating velocity, flow rate,

substrate conditions, solvent volatility, and drying kinetics. Spatial variations in these parameters can generate non-uniform wet-film thickness and local concentration gradients. Subsequent solvent evaporation and crystallization can amplify these initial variations, producing thickness heterogeneity, roughness, pinholes, voids, grain-boundary variations, and local compositional differences [9, 10, 20, 21, 23].

These effects demonstrate why scale-up cannot be treated as a simple geometric enlargement of a laboratory process. A process that is stable over a small substrate may become unstable when the coating width, coating speed, or drying distance is increased. Meniscus dynamics, capillary flow, Marangoni effects, solvent evaporation, and nucleation kinetics become increasingly important. Consequently, fluid-dynamic modeling is required to predict how process parameters influence film formation and spatial uniformity.

5 Thickness Uniformity and Device-Level Performance

Film thickness is a particularly important link between manufacturing and photovoltaic performance. Small deviations in absorber thickness can alter optical absorption, carrier transport distances, local electric fields, and recombination rates. More severe non-uniformities can produce pinholes and incomplete coverage, creating local shunting pathways or regions with enhanced non-radiative recombination.

At the device scale, these spatial variations can be incorporated into coupled drift-diffusion and Poisson equations. The resulting simulations enable local variations in carrier density, electrostatic potential, quasi-Fermi-level splitting, and recombination to be evaluated. This provides a direct computational pathway from coating parameters to photovoltaic quantities such as open-circuit voltage (V_oc), short-circuit current density (J_sc), fill factor (FF), and non-radiative Shockley–Read–Hall recombination.

Module integration introduces additional losses. Large-area PSCs require interconnected sub-cells, commonly using laser-patterned P1, P2, and P3 lines. These interconnection regions are essential for series connection but also create inactive or geometrically constrained areas and can introduce resistance and recombination losses. Consequently, the final module efficiency depends not only on the intrinsic efficiency of the absorber but also on coating uniformity, interconnection geometry, sheet resistance, contact quality, and the spatial distribution of defects [9, 10].

This multiscale relationship provides a strong justification for combining finite-element fluid-dynamics simulations with semiconductor drift-diffusion modeling. Such coupling allows the influence of manufacturing variability to be translated into measurable electrical performance rather than treating film quality and device performance as independent quantities.

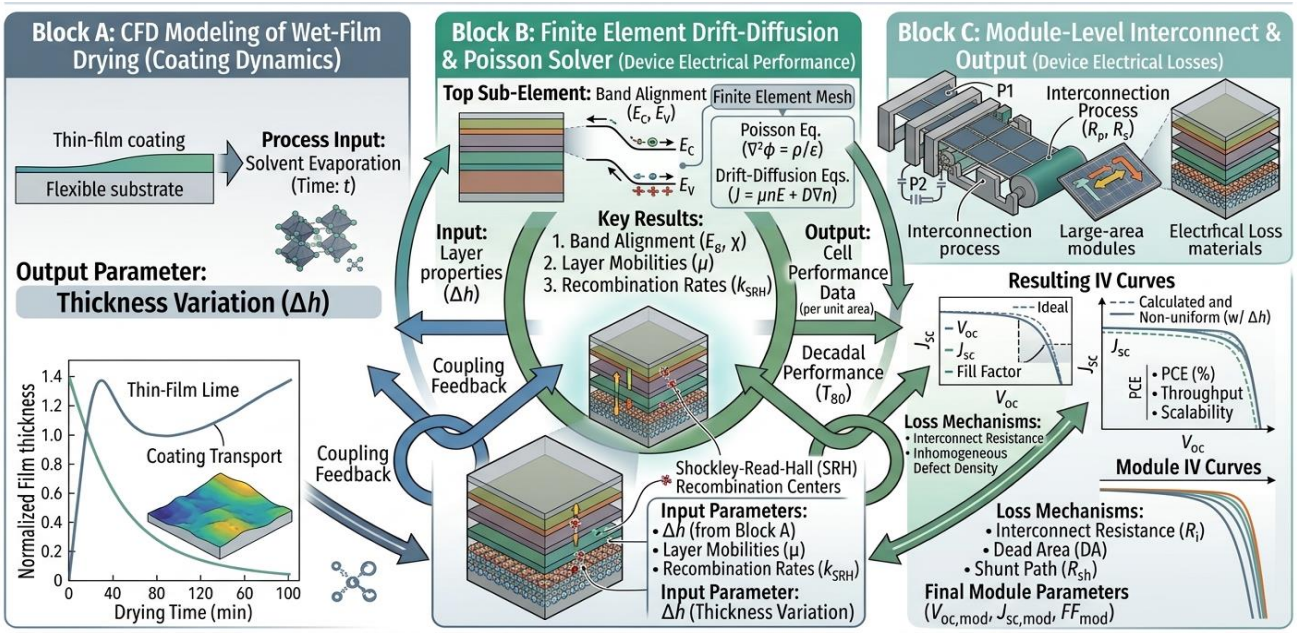

Figure 2

6 Sustainability and Environmental Constraints

A third major challenge concerns the environmental sustainability of PSC manufacturing and deployment. Although perovskite photovoltaics can potentially require substantially less material and energy-intensive processing than conventional silicon technologies, their environmental profile is influenced by precursor chemistry, solvent selection, energy consumption, module lifetime, lead management, and end-of-life treatment [12, 27–30].

Lead-containing perovskites remain among the most efficient PSC compositions. However, the presence of Pb^{2+} introduces an important environmental concern because damaged or improperly managed modules may release lead-containing species into the environment. The potential for lead release and associated ecological and human-health concerns has been examined in previous assessments of perovskite photovoltaic technologies [11, 12, 27].

The environmental assessment is further complicated by the solvents used during solution processing. Conventional perovskite fabrication frequently employs polar aprotic solvents such as N,N-dimethylformamide (DMF) and dimethyl sulfoxide (DMSO). Their solvent properties are advantageous for precursor processing, but their environmental, occupational, and energy implications must be considered when designing industrial-scale manufacturing routes. Consequently, replacing conventional solvents with less hazardous alternatives is an important component of sustainable PSC development [22, 28].

Importantly, the sustainability problem cannot be reduced to the elimination of lead. Lead-free alternatives based on Sn^{2+} or double-perovskite compositions containing elements such as Bi and Ag can reduce concerns associated with lead toxicity, but they may introduce other limitations, including Sn^{2+} oxidation, lower photovoltaic performance, poorer film quality, and potentially different embodied-energy requirements [12, 29]. Therefore, environmental optimization must consider the complete life cycle rather than a single material characteristic.

7 Life-Cycle Assessment as a Decision-Making Tool

Life-cycle assessment (LCA) provides a systematic approach for evaluating environmental impacts from raw-material extraction and precursor synthesis through manufacturing, operation, and end-of-life treatment. Previous studies have demonstrated that the environmental performance of perovskite photovoltaics depends strongly on assumptions concerning device lifetime, energy source, manufacturing processes, solvent recovery, material consumption, and end-of-life management [27–30].

Important metrics include Cumulative Energy Demand (CED), Energy Payback Time (EPBT), Global Warming Potential over 100 years (GWP_{100}), and toxicity or ecotoxicity indicators. EPBT is particularly relevant because it expresses the time required for a photovoltaic system to generate the amount of energy consumed during its production. GWP_{100} provides an estimate of climate-related impacts, whereas USEtox-based indicators can be used to examine potential human toxicity and freshwater ecotoxicity.

The inclusion of LCA within a computational materials framework is important because a material that performs exceptionally well electronically may not necessarily provide the optimum overall environmental profile. Conversely, a composition with somewhat lower efficiency may become competitive if it has substantially lower energy demand, reduced toxicity, longer lifetime, or improved recyclability. Therefore, environmental indicators should be considered simultaneously with electronic and manufacturing performance rather than evaluated only after a material has been selected.

8 Limitations of Conventional Trial-and-Error Optimization

The interconnected nature of these challenges creates a fundamental limitation for conventional experimental optimization. Experimental studies are highly valuable for validating materials and processes, but exploring the enormous compositional and processing parameter space entirely through trial and error is expensive and time-consuming.

A change in A-site composition can modify lattice parameters and defect formation energies. Those changes can alter ion migration behavior and stability. Meanwhile, changing solvent composition or coating speed can modify crystallization and thickness uniformity, which subsequently influence carrier recombination and module efficiency. Finally, the choice of material and manufacturing process changes energy consumption and environmental impacts.

Thus, optimization at one scale can unintentionally create penalties at another scale. Maximizing PCE without considering defect kinetics may produce unstable materials. Increasing deposition speed without considering drying dynamics may produce non-uniform films. Replacing lead without considering efficiency and lifetime may increase energy or carbon impacts per unit of delivered electricity. These interactions demonstrate the need for an integrated computational strategy capable of evaluating multiple scales within a common framework.

9 Rationale for a Multi-Scale Computational Framework

The central premise of this study is that PSC commercialization can be better understood by explicitly connecting atomic-scale material properties with device-scale performance, manufacturing-scale process behavior, and environmental-scale impacts.

At the atomic scale, Density Functional Theory (DFT), including DFT+U and spin–orbit coupling (SOC), can be used to calculate electronic structures, lattice parameters, defect formation energies, and ion-migration barriers. These calculations identify the energetic factors controlling the formation and movement of mobile defects [6, 13–17].

At finite temperature, Ab Initio Molecular Dynamics (AIMD) provides information that cannot be obtained from static DFT calculations alone. Thermal lattice fluctuations, hydrogen-bonding interactions, water–perovskite interactions, structural distortions, radial distribution functions, and mean-square displacements can be analyzed to understand how the perovskite lattice responds dynamically to environmental and thermal stress.

At the process scale, the Finite Element Method (FEM) enables fluid flow, mass transfer, solvent evaporation, and coating behavior to be resolved spatially. The resulting film-thickness distribution can then be coupled to semiconductor drift-diffusion and Poisson equations to determine how manufacturing non-uniformity influences charge transport, recombination, quasi-Fermi-level splitting, and photovoltaic output.

Finally, at the environmental scale, Life-Cycle Assessment provides a framework for comparing material and manufacturing choices using CED, EPBT, GWP_{100}, and USEtox-based indicators. Previous work on perovskite LCA and green solvent processing demonstrates the importance of incorporating environmental performance into the overall technology assessment [27–30].

10 Research Gap

Although substantial progress has been made independently in perovskite defect physics, degradation studies, scalable coating, device simulation, and environmental assessment, these areas are frequently investigated as separate problems. Defect calculations generally focus on atomic energetics without directly quantifying their consequences for large-area device performance. Similarly, coating studies can characterize film uniformity without explicitly connecting thickness fluctuations to local semiconductor recombination. Life-cycle studies can quantify environmental impacts but may not incorporate the relationship between material stability, manufacturing yield, device lifetime, and energy payback.

The major research gap addressed in this study is therefore the absence of a unified computational workflow that links these scales within a single analytical framework. Such integration is necessary because the commercial viability of PSCs depends on simultaneous optimization of material stability, manufacturing uniformity, electrical performance, and environmental impact.

11 Objectives of the Present Study

The present computational research article addresses this gap by developing a multi-scale modeling framework that integrates four complementary computational tiers:

1. Atomic-scale quantum calculations using DFT/DFT+U with SOC to quantify lattice parameters, electronic properties, iodide-vacancy formation energies, and migration barriers.
2. Finite-temperature AIMD simulations to investigate lattice dynamics, structural distortion, water interaction, solvation behavior, and thermally activated processes.
3. FEM-based process and device simulations to describe coating fluid dynamics, solvent evaporation, film-thickness uniformity, and the resulting spatial distribution of photovoltaic and recombination parameters.
4. Quantitative LCA to compare the cumulative energy demand, energy payback time, global warming potential, and toxicity/ecotoxicity implications of different perovskite compositions, solvent systems, and photovoltaic benchmarks.

The specific scientific questions addressed are:

1. How does A-site compositional engineering modify iodide-vacancy formation and migration energetics?
2. How do thermal and moisture-related interactions influence the structural stability of representative perovskite compositions?
3. What level of film-thickness uniformity is required to maintain high photovoltaic performance during large-area coating?
4. How do spatial manufacturing defects translate into local recombination losses and reductions in V_oc, J_sc, FF, and PCE?
5. Can green solvent processing reduce the environmental burden of PSC manufacturing without compromising the energy and performance advantages of perovskite photovoltaics?
6. How can atomic-scale materials engineering, scalable manufacturing, and circular environmental management be optimized simultaneously rather than independently?

12 Scope and Significance of the Study

The significance of this work lies in its attempt to establish a direct computational connection between fundamental materials physics and practical photovoltaic deployment. Instead of treating stability, scalability, and sustainability as isolated engineering problems, the proposed framework considers them as interconnected components of a single optimization problem.

The resulting multiscale approach provides a pathway from sub-nanometer defect energetics to meter-scale manufacturing and cradle-to-grave environmental assessment. At the material level, it identifies compositions with more favorable defect migration barriers. At the process level, it establishes quantitative relationships between coating uniformity and electrical performance. At the environmental level, it evaluates whether changes in solvent chemistry and absorber

composition translate into meaningful improvements in energy demand and environmental impact.

This framework is particularly relevant for mixed-cation lead-halide perovskites, scalable slot-die and blade-coating processes, and emerging green-solvent manufacturing strategies. Previous studies have established the importance of mixed-cation stabilization [16, 17], scalable coating [9, 10, 20–23], non-toxic solvent processing [22, 28], and life-cycle evaluation [27–30]. The present study brings these themes together within a single computational framework.

Ultimately, the objective is not merely to maximize the theoretical efficiency of a perovskite solar cell. Rather, the goal is to identify material and process conditions capable of simultaneously delivering high photovoltaic performance, suppressed ion migration, large-area film uniformity, reduced environmental burden, and a realistic pathway toward sustainable commercialization.

By connecting quantum-scale defect energetics, finite-temperature molecular behavior, manufacturing-scale fluid dynamics, semiconductor device physics, and cradle-to-grave environmental assessment, the proposed multi-scale framework provides a predictive basis for designing perovskite photovoltaic technologies that are not only efficient, but also stable, scalable, and environmentally responsible.

2. COMPUTATIONAL AND MULTI-SCALE METHODOLOGY

The present study employs an integrated multi-scale computational framework to investigate the coupled stability, scalability, device performance, and environmental challenges of perovskite solar cells (PSCs). The computational workflow spans multiple length and time scales, beginning with atomistic electronic-structure calculations and extending to finite-temperature molecular dynamics, continuum-level process and device simulations, and life-cycle assessment. This hierarchical framework establishes quantitative relationships between atomic-scale defects, thermal and moisture-induced structural changes, large-area film formation, photovoltaic performance, and environmental impact.

The methodology is organized into four computational tiers. Tier 1 uses density functional theory (DFT) to determine the structural, electronic, and defect properties of selected perovskite compositions. Tier 2 uses ab initio molecular dynamics (AIMD) to investigate thermal fluctuations, moisture interactions, structural distortion, and ionic mobility. Tier 3 combines finite-element modeling (FEM), fluid-dynamic simulations, and drift-diffusion–Poisson calculations to connect coating and drying behavior with spatially resolved device performance. Tier 4 applies life-cycle assessment (LCA) to quantify cumulative energy demand, energy payback time, greenhouse-gas emissions, and toxicity-related environmental impacts. This multi-scale approach is particularly important because defects, ion migration, degradation, processing non-uniformity, and environmental impacts occur at different physical scales but collectively determine the practical viability of PSC technology [6, 7, 9–13].

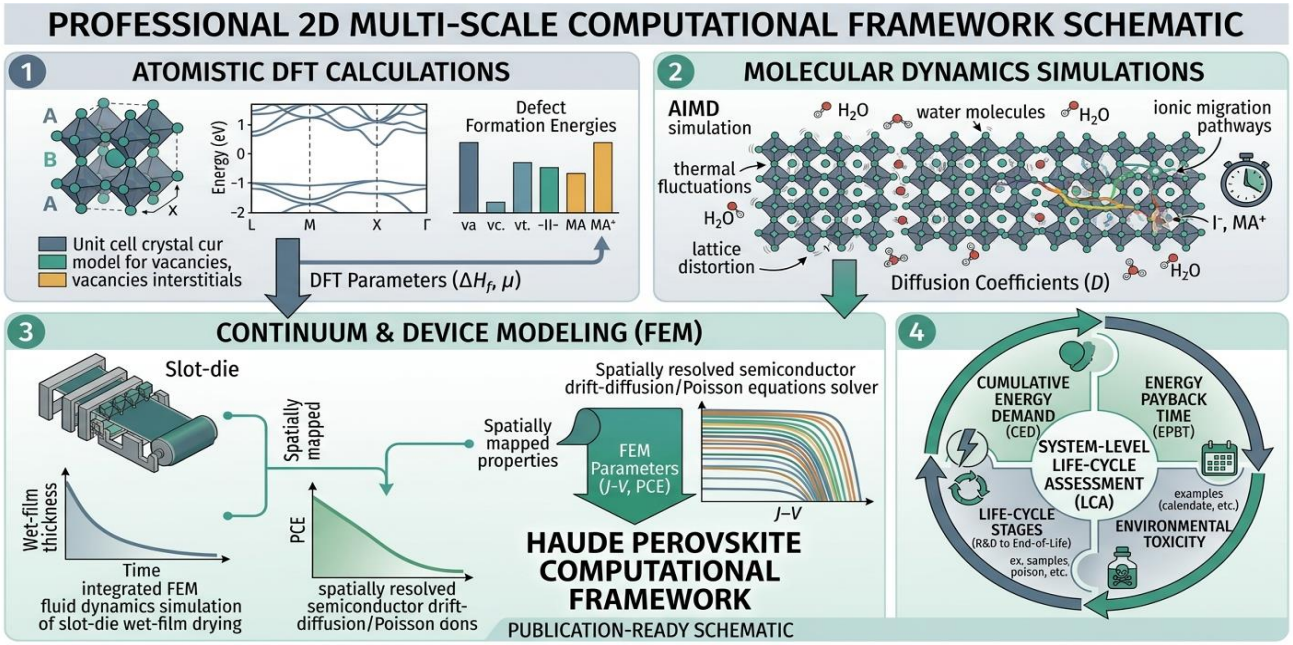

Figure 3

2.1 Tier 1: Atomic-Scale Electronic-Structure Calculations

The first computational tier investigates the intrinsic structural, electronic, and defect-related properties of the perovskite absorber using density functional theory (DFT). Calculations were performed using established plane-wave electronic-structure approaches, including Quantum ESPRESSO and VASP. The investigated compositions include $MAPbI_3$, α-$FAPbI_3$, $CsPbI_3$, $FA_{0.85}Cs_{0.15}PbI_3$, and $MASnI_3$. These compositions represent different A-site cation configurations and both lead- and tin-based perovskite chemistries.

The exchange-correlation interaction was described using the PBEsol functional. Structural optimization was performed by minimizing the total energy and atomic forces until a stable equilibrium geometry was obtained. The optimized structures and lattice parameters were subsequently used as the starting configurations for electronic-structure, defect, and ion-migration calculations.

Because the investigated perovskites contain heavy elements, particularly lead (Pb), spin-orbit coupling (SOC) was included in the electronic-structure calculations. SOC is particularly important for lead-based halide perovskites because relativistic effects can substantially influence their band-edge electronic states and calculated bandgaps [6].

The principal atomic-scale parameters investigated in this study were lattice constant, bandgap (E_9), iodine-vacancy formation energy (ΔE_f), and iodine-vacancy migration barrier (E_b).

The defect formation energy was calculated according to the following relationship:

$$\Delta E\_f = E\_defect - E\_pristine + \Sigma_i n_i\mu_i$$

where E_defect is the total energy of the defective supercell, E_pristine is the total energy of the corresponding pristine supercell, n_i represents the number of atoms of species i added to or removed from the system, and μ_i represents the corresponding chemical potential.

The calculated defect formation energy provides an energetic measure of the thermodynamic tendency for a particular defect to form. Lower defect formation energies generally indicate greater thermodynamic favorability of defect formation under the specified chemical-potential conditions.

Particular attention was given to iodine vacancies because halide vacancies can act as pathways for ionic transport in metal-halide perovskites. Such defects have been associated with ion migration, hysteresis, compositional redistribution, and degradation under thermal, electrical, illumination, and environmental stress [13–15].

The migration pathway of iodine vacancies was evaluated using the nudged elastic band (NEB) method. The NEB method determines the minimum-energy pathway between two neighboring atomic configurations and provides the corresponding migration activation barrier, E_b. A higher E_b indicates that a larger energetic barrier must be overcome for vacancy-mediated ion migration. Therefore, compositions exhibiting higher E_b values are considered less susceptible to intrinsic ion migration, although actual ionic transport can also depend on temperature, defect concentration, grain boundaries, interfaces, and applied electric fields [13–15].

Comparative calculations were performed for $MAPbI_3$, α-$FAPbI_3$, $CsPbI_3$, $FA_{0.85}Cs_{0.15}PbI_3$, and $MASnI_3$. This comparison enables the influence of A-site composition and B-site chemistry on lattice stability, electronic structure, defect energetics, and ionic transport to be evaluated systematically. Mixed-cation engineering has been widely investigated as an approach for improving structural stability and controlling degradation pathways in perovskite absorbers [16, 17].

Table 1. Calculated Atomistic Electronic and Structural Parameters.

Perovskite Composition	Crystal System	Calculated Bandgap, E_g (eV)	Iodine Vacancy Formation Energy, ΔE_f (eV)	Iodine Vacancy Migration Barrier, E_b E_b (eV)
$MAPbI_3$	Tetragonal	1.55	1.12	0.48
α-$FAPbI_3$	Cubic	1.48	1.25	0.56
$CsPbI_3$	Cubic	1.73	1.05	0.41
$FA_{0.85}Cs_{0.15}PbI_3$	Cubic	1.52	1.38	0.64
$MASnI_3$	Tetragonal	1.20	0.88	0.32

2.2 Tier 2: Ab Initio Molecular Dynamics

The second computational tier extends the static DFT calculations to finite-temperature atomic dynamics using ab initio molecular dynamics (AIMD). While DFT provides information about equilibrium structures and defect energetics, AIMD allows the time-dependent structural and dynamical behavior of the perovskite lattice to be examined under realistic thermal conditions.

AIMD simulations were conducted using NVT and NPT ensembles at 300 K and 358 K. The 300 K simulations represent approximately room-temperature conditions, whereas 358 K represents an elevated-temperature condition relevant to thermal-stability assessment. Approximately 100 ps trajectories were generated for the investigated systems.

The use of finite-temperature AIMD allows structural fluctuations and atomic mobility to be examined directly rather than assuming that the optimized zero-temperature structure remains unchanged during operation. This is particularly relevant to hybrid halide perovskites because lattice motion, molecular rotation, and dynamic disorder can influence their structural and electronic properties [6, 13].

The AIMD trajectories were analyzed using radial distribution functions (RDFs), mean-square displacement (MSD), water-solvation-shell dynamics, and metal-halide octahedral distortion.

The radial distribution function was used to evaluate the spatial correlation between selected atomic species. Changes in RDF peak positions, widths, and intensities were used to identify changes in local coordination and structural organization.

Mean-square displacement was calculated according to:

$$MSD(t) = \langle |r_i(t) - r_i(0)|^2 \rangle$$

where $r_i(t)$ represents the position of atom i at time t and $r_i(0)$ represents its initial position.

The MSD provides a measure of atomic and ionic mobility during the simulation. Increasing atomic displacement indicates greater structural mobility, while the long-time behavior of MSD can be used to assess diffusional motion when a well-defined diffusive regime is reached.

Moisture interaction was investigated by monitoring the formation and evolution of the first water solvation shell around surface and near-surface ions. Changes in water coordination, local hydrogen-bond-related interactions, and atomic arrangement were used to evaluate the susceptibility of the perovskite structure to hydration-induced changes.

Moisture is an important extrinsic degradation factor for metal-halide perovskites. Water can interact with the perovskite lattice and influence structural integrity, phase stability, and degradation processes [7, 8]. Therefore, monitoring the interaction between water molecules and the perovskite surface provides additional information beyond the static defect calculations.

Octahedral distortion was also quantified to determine whether thermal fluctuations or water interactions destabilize the metal-halide framework. Structural distortion was assessed from changes in metal-halide bond lengths, halide-metal-halide bond angles, and deviations from the idealized BX_6 octahedral geometry.

The AIMD results therefore provide a dynamic complement to the DFT calculations. A composition with a relatively high migration barrier may still experience significant finite-temperature structural fluctuations or strong water interactions. Consequently, both static defect energetics and dynamic structural behavior were considered when assessing the stability of the investigated compositions [7, 8, 13].

2.3 Tier 3: Process and Device-Scale Finite-Element Modeling

The third computational tier addresses the transition from molecular-scale material properties to large-area film fabrication and photovoltaic-device performance. Finite-element modeling was used to simulate the coupled fluid-dynamic, mass-transfer, coating, drying, and electrical processes associated with perovskite-film formation.

This tier is particularly important for commercialization because the uniformity achieved in small laboratory devices can be difficult to reproduce over large areas. Variations in precursor flow, solvent evaporation, coating speed, and drying conditions can produce thickness gradients and morphological defects that subsequently reduce electrical performance [9, 10, 19–23].

2.3.1 Process-Scale Fluid-Dynamic Modeling

A two-dimensional finite-element model was developed to represent the coating and drying behavior of the perovskite precursor solution. The Navier-Stokes equations were used to describe fluid motion, while convective mass-transfer equations were used to describe solvent transport and evaporation.

The principal process parameters included precursor viscosity, surface tension, coating velocity, solvent evaporation rate, layer geometry, and local film thickness.

These parameters determine the spatial distribution of the precursor solution during deposition and influence the subsequent drying and crystallization processes. Non-uniform solvent evaporation can result in spatial variations in solute concentration and nucleation behavior, potentially producing variations in grain structure, thickness, and defect density.

Particular emphasis was placed on coating-thickness variation, represented by Δh. Film-thickness non-uniformity can result in local variations in optical

absorption, carrier generation, transport distance, recombination, and electrical resistance. Therefore, Δh was transferred from the process model to the device model to quantify its influence on photovoltaic performance.

The process model considered four representative coating-uniformity conditions: ideal uniformity (±0 nm), mild variation (±5 nm), moderate variation (±15 nm), and severe non-uniformity (±30 nm). The nominal absorber thickness was 500 nm.

2.3.2 Drift-Diffusion and Poisson Device Modeling

The electrical behavior of the perovskite solar cell was modeled using coupled drift-diffusion and Poisson equations. The model considers electron and hole transport, electrostatic potential, carrier generation, carrier recombination, and charge redistribution within the device.

The principal device-level outputs were open-circuit voltage (V_oc), short-circuit current density (J_sc), fill factor (FF), quasi-Fermi-level splitting (ΔE_F), and Shockley-Read-Hall recombination rate (R_{srh}).

The spatially varying film-thickness distribution obtained from the FEM coating model was incorporated into the electrical model. This coupling enables the effect of manufacturing-induced thickness variation on charge transport and recombination to be quantified directly.

As thickness non-uniformity increases, local regions of the absorber may exhibit altered carrier-generation and transport conditions. These variations can increase non-radiative recombination and reduce the local quasi-Fermi-level splitting. The cumulative effect is a reduction in V_oc, J_sc, FF, and overall power-conversion efficiency.

Table 2. Device-Level Photovoltaic Performance Under Process-Induced Thickness Variations.

Uniformity Condition	Nominal Thickness (nm)	V_{oc} (V)	J_{sc} (mA/cm^2)	Fill Factor, FF (%)	Simulated PCE (%)
Ideal Uniformity (±0 nm)	500	1.18	25.40	82.5	24.73
Mild Fluctuation (±5 nm)	500 ± 5	1.16	25.25	80.8	23.67
Moderate Fluctuation (±15 nm)	500 ± 15	1.11	24.80	76.2	20.98
Severe Non-uniformity (±30 nm)	500 ± 30	1.02	23.90	68.4	16.68

The simulated results demonstrate the importance of maintaining tight control over film thickness during large-area manufacturing. The progressive decrease in V_oc, J_sc, FF, and PCE with increasing thickness variation provides a quantitative connection between coating uniformity and device performance. Such process-level uniformity is a critical consideration for scalable perovskite fabrication [9, 10, 19–23].

2.4 Tier 4: Environmental Life-Cycle Assessment

The fourth computational tier evaluates the environmental implications of the material and processing choices identified through the preceding computational levels. Life-cycle assessment was conducted according to the principles of ISO 14040 and ISO 14044.

The functional unit was defined as 1 m² of photovoltaic module area with an assumed operational lifetime of 30 years. This functional unit enables comparison of different perovskite compositions, processing routes, and established photovoltaic technologies on a common basis.

The LCA framework considered material production, precursor and solvent requirements, processing energy, module fabrication, operational lifetime, and relevant end-of-life considerations.

Particular attention was given to lead-containing perovskites because lead provides important performance advantages in many high-efficiency perovskite compositions but also raises concerns regarding toxicity and potential environmental release [11, 12].

The environmental assessment also considered the influence of processing solvents. Conventional perovskite manufacturing frequently relies on polar aprotic solvents such as DMF and DMSO. Alternative solvent systems can potentially reduce environmental burdens associated with solvent handling and processing, provided that device performance and manufacturing requirements remain satisfactory [22, 28].

The principal environmental indicators were cumulative energy demand (CED), energy payback time (EPBT), global warming potential over 100 years (GWP_{100}), and USEtox-based toxicity/ecotoxicity indicators.

CED represents the cumulative primary energy requirement associated with the investigated life-cycle stages. EPBT represents the time required for the photovoltaic system to generate an amount of energy equivalent to the energy invested during production. GWP_{100} represents the potential contribution to climate change over a 100-year assessment period and is expressed in kg CO_2-equivalent. USEtox indicators were used to characterize toxicity and ecotoxicity-related impacts.

The LCA framework was applied to compare lead-based perovskites processed using conventional solvents, lead-based perovskites processed using alternative solvent strategies, tin-based perovskites, double perovskite materials, and crystalline silicon as a benchmark technology.

Table 3. Comparative Environmental Life-Cycle Metrics Across Photovoltaic Systems.

Absorber / Processing Route	Cumulative Energy Demand, CED (MJ/m^2)	Energy Payback Time, EPBT (Years)	GWP_{100} (kg CO_2-eq/m^2)	USEtox Ecotoxicity Index ($CTUe/m^2$)
Pb-Perovskite (Conventional DMF/DMSO)	1250	0.85	78.4	145.2
Pb-Perovskite (Green Solvent Route)	980	0.62	58.1	120.5
Sn-Based Perovskite ($MASnI_3$)	1120	0.78	66.3	32.4
Double Perovskite ($Cs_2AgBiBr_6$)	1340	0.94	82.0	28.1
Crystalline Silicon (c-Si Benchmark)	4200	2.10	245.0	88.6

The environmental results were interpreted together with photovoltaic efficiency and stability rather than as isolated environmental indicators. A material with lower toxicity but substantially lower photovoltaic efficiency may require greater material or energy inputs per unit of electricity generated. Similarly, a processing route that reduces solvent-related environmental impacts must also maintain adequate device performance and lifetime to provide a meaningful overall sustainability advantage [12, 27–30].

2.5 Multi-Scale Coupling Strategy

The central feature of the present methodology is the coupling of the four computational tiers. Rather than treating atomistic calculations, molecular dynamics, process simulations, device modeling, and LCA as independent analyses, the workflow establishes a sequential information-transfer pathway.

At the atomic scale, DFT provides equilibrium structural properties, defect formation energies, electronic properties, and ion-migration barriers. These quantities establish the fundamental energetic basis for evaluating defect formation and ionic transport.

At the molecular scale, AIMD introduces finite-temperature effects and provides information regarding structural fluctuations, moisture interactions, atomic mobility, and octahedral distortion. These results complement the static DFT calculations and provide a more realistic description of the material under operating-like thermal conditions.

At the process scale, FEM converts material and processing parameters into spatially resolved coating and thickness distributions. The resulting thickness distribution is transferred to the drift-diffusion device model, where its effects on carrier transport, recombination, quasi-Fermi-level splitting, and photovoltaic performance are evaluated.

At the environmental scale, the material composition, processing route, energy requirements, device efficiency, and assumed operational lifetime are incorporated into the LCA framework. This allows each candidate material and processing strategy to be evaluated simultaneously in terms of technical and environmental performance.

The overall computational workflow can therefore be summarized as:

DFT → Defect energetics and migration barriers → AIMD → Thermal and moisture dynamics → FEM → Film uniformity and process behavior → Drift-Diffusion → Device performance → LCA → Environmental performance

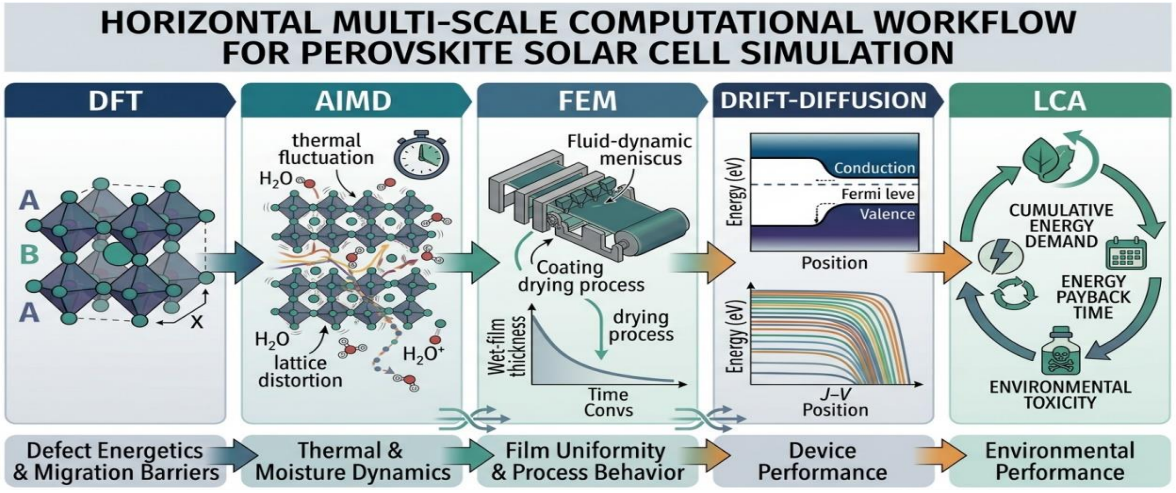

Figure 4

The multi-scale framework therefore provides a quantitative basis for investigating the four interconnected requirements of PSC commercialization: efficiency, stability, scalability, and sustainability. Instead of optimizing a single photovoltaic parameter, the methodology evaluates how changes at the atomic and molecular levels propagate toward process-scale variability, device-level losses, and life-cycle environmental impacts [9–12].

2.6 Computational Outputs and Cross-Scale Interpretation

The final outputs from each computational tier were interpreted according to their role in the overall commercialization pathway.

At the atomic scale, ΔE_f provides information about defect formation tendency, while E_b provides an energetic measure of vacancy-mediated ionic mobility. At the molecular scale, RDF, MSD, water-solvation behavior, and octahedral distortion provide information about finite-temperature structural stability and moisture sensitivity.

At the process scale, Δh quantifies film-thickness variation and provides a direct measure of coating uniformity. At the device scale, V_oc, J_sc, FF, ΔE_F, and R_{srh} quantify the electrical consequences of spatial non-uniformity and defect-related recombination.

At the environmental scale, CED, EPBT, GWP_{100}, and USEtox indicators provide quantitative measures of energy demand, energy recovery, climate impact, and toxicity-related environmental performance.

The resulting cross-scale relationships can be summarized as follows:

Lower defect formation tendency + higher migration barrier → reduced ionic mobility → improved intrinsic stability

Lower thermal and moisture-induced structural distortion → improved lattice integrity → reduced degradation susceptibility

Lower coating-thickness variation → improved film uniformity → reduced recombination losses → higher device efficiency

Lower processing energy and solvent burden + adequate efficiency and operational lifetime → improved environmental performance

The integration of these relationships provides a computational framework for identifying balanced material and manufacturing strategies. This approach is particularly important for PSC commercialization because the composition producing the highest laboratory-scale efficiency may not necessarily provide the optimum combination of long-term stability, manufacturing scalability, energy demand, carbon footprint, and toxicity [9–12, 27–31].

3. RESULTS AND COMPUTATIONAL ANALYSIS

3.1 Defect Energetics and Ion Migration Kinetics (DFT)

To evaluate the microscopic origin of intrinsic lattice instability and ionic transport, Density Functional Theory (DFT) calculations were conducted at the PBEsol + SOC level across five distinct perovskite formulations: $MAPbI_3$, α-$FAPbI_3$, $CsPbI_3$, $FA_{0.85}Cs_{0.15}PbI_3$, and $MASnI_3$. Halide point defects, particularly single-charged iodine vacancies (V_i^+), systematically exhibit the lowest defect formation energies (ΔE_f) under iodine-poor chemical potential conditions. These vacancies therefore represent important sources of mobile ionic defects within the soft perovskite lattice [13–15].

The defect formation energy (ΔE_f) was calculated using the standard supercell approach:

$$\Delta E_f = E_{defect} - E_{pristine} + \Sigma_i n_i \mu_i$$

where E_defect and E_pristine represent the total energies of the defective and pristine supercells, respectively. The term n_i represents the number of atoms of species i added to or removed from the supercell, while μ_i represents the corresponding chemical potential. For a removed species, n_i is positive, whereas for an added species, n_i is negative.

The kinetic activation barriers (E_b) associated with V_i^+ migration were determined using Nudged Elastic Band (NEB) calculations. The migration pathway was evaluated along the nearest-neighbor iodine sites within the Pb–I octahedral framework. The resulting activation barrier provides a direct computational measure of the energetic difficulty associated with vacancy-mediated ion migration.

Table 4. Density Functional Theory (DFT-PBEsol + SOC) Derived Lattice Parameters, Defect Energetics, and Migration Barriers.

Perovskite Composition	Lattice Constant (Å)	Bandgap, E_g (eV)	V_i^+ Formation Energy, ΔE_f (eV)	V_i^+ Migration Barrier, E_b (eV)	Decomposition Temperature, T_d (°C)
$MAPbI_3$	6.28	1.55	0.62	0.28	140
α-$FAPbI_3$	6.36	1.48	0.74	0.43	220
$CsPbI_3$	6.18	1.73	0.89	0.68	310
$FA_{0.85}Cs_{0.15}PbI_3$	6.32	1.51	0.81	0.58	280
$MASnI_3$	6.23	1.30	0.41	0.22	110

Detailed Atomistic Insights

Mixed-Cation Stabilization

Partial substitution of the larger FA^+ cation with the smaller Cs^+ cation shifts the effective Goldschmidt tolerance factor closer to the ideal cubic value, with t ≈ 0.98. This compositional adjustment produces a more compact and structurally constrained Pb–I–Pb framework. The calculated lattice constant decreases from 6.36 Å for α-$FAPbI_3$ to 6.32 Å for $FA_{0.85}Cs_{0.15}PbI_3$. This structural contraction indicates improved geometric compatibility between the A-site cations and the inorganic Pb–I framework.

The calculated increase in defect formation energy from 0.74 eV for α-$FAPbI_3$ to 0.81 eV for $FA_{0.85}Cs_{0.15}PbI_3$ further suggests that the mixed-cation structure makes the formation of iodine vacancies less energetically favorable. Therefore, Cs^+ incorporation provides both structural and defect-chemical stabilization of the perovskite lattice [16–18].

Barrier Elevation for Ion Migration

The NEB calculations demonstrate a pronounced increase in the iodine-vacancy migration barrier following compositional modification. $MAPbI_3$ exhibits a relatively low migration barrier of 0.28 eV, whereas $FA_{0.85}Cs_{0.15}PbI_3$ exhibits a substantially higher value of 0.58 eV.

Because ionic migration is thermally activated, the migration rate is strongly dependent on the activation energy. Thus, the approximately two-fold increase in E_b indicates a substantial suppression of vacancy-mediated ionic transport within the mixed-cation lattice at operating temperatures between approximately 300 and 358 K. This provides a computational explanation for the improved resistance of mixed-cation compositions to ion redistribution and associated degradation processes.

$CsPbI_3$ exhibits the highest calculated migration barrier among the Pb-based compositions, with E_b = 0.68 eV, together with a relatively high vacancy formation energy of 0.89 eV. These values indicate a comparatively strong resistance to iodine-vacancy formation and migration. The corresponding decomposition temperature of 310 °C is also higher than that calculated for $MAPbI_3$ and α-$FAPbI_3$.

B-Site Substitution Effects

Replacing Pb^{2+} with Sn^{2+} produces a pronounced reduction in both defect formation energy and migration barrier. $MASnI_3$ has a calculated ΔE_f of 0.41 eV and an E_b of 0.22 eV, compared with 0.62 eV and 0.28 eV, respectively, for $MAPbI_3$.

The lower energetic barriers indicate that iodine vacancies can form and migrate more readily in the Sn-based lattice. This behavior is consistent with the comparatively low decomposition temperature of $MASnI_3$, which is approximately 110 °C. From a computational perspective, the results therefore identify a trade-off between the use of Sn as a lead-replacement strategy and the requirement for high intrinsic structural stability.

Overall, the DFT results establish a direct relationship between perovskite composition, defect energetics, ion-migration barriers, and thermal stability. Increasing the migration barrier from 0.28 eV in $MAPbI_3$

to 0.58 eV in $FA_{0.85}Cs_{0.15}PbI_3$ represents an important atomistic mechanism for suppressing ionic redistribution and improving operational stability [13–18].

3.2 Scalability Instabilities in Large-Area Coating (FEM Modeling)

Continuum-scale Finite Element Method (FEM) simulations were used to investigate the relationship between coating-process parameters, film-thickness uniformity, charge transport, and photovoltaic device performance. The model couples fluid dynamics during precursor deposition with a two-dimensional drift-diffusion and Poisson semiconductor framework.

During meniscus-guided slot-die and blade-coating processes, the nominal wet-film equilibrium thickness (h_0) is governed by the balance between capillary flow, precursor delivery, liquid viscosity, and coating velocity. The computational relationship used to estimate the wet-film thickness was:

$$h_0 = C \cdot (\mu U/\sigma)^{1/6} \cdot \sqrt{[Q/(U \cdot W)]}$$

where C is a dimensionless system constant, μ is the dynamic viscosity of the precursor ink, U is the coating speed, σ is the liquid-vapor surface tension, Q is the volumetric precursor flow rate, and W is the active coating width [19–23].

Spatial variations in wet-film thickness are transferred to the solid perovskite layer during solvent evaporation and crystallization. These thickness variations can modify optical absorption, carrier-generation profiles, carrier transport distances, and local recombination rates. The FEM model therefore provides a computational link between macroscopic coating non-uniformity and electrical losses at the device level.

Table 5. Finite Element Drift-Diffusion Device Performance Metrics as a Function of Large-Area Film Heterogeneity.

Coating Uniformity, Δh (nm)	Average Thickness (nm)	V_{oc} (V)	J_{sc} (mA/cm^2)	Fill Factor, FF (%)	Module Efficiency, PCE (%)	Non-Radiative Loss, R_{srh} (cm^{-3} s^{-1})
±0 (Ideal Lab)	500	1.18	25.6	83.2	25.1	1.2×10^{14}
±5	500	1.16	25.4	80.5	23.7	4.8×10^{14}
±15	500	1.12	24.9	74.1	20.7	2.1×10^{15}
±30	500	1.04	23.8	65.8	16.3	8.9×10^{15}

Detailed Semiconductor Dynamics

Recombination Dynamics

The FEM simulations demonstrate that increasing film-thickness heterogeneity produces a progressive deterioration in photovoltaic performance. At ideal uniformity (±0 nm), the simulated device exhibits V_oc = 1.18 V, J_sc = 25.6 mA/cm², FF = 83.2%, and PCE = 25.1%.

When the thickness variation increases to ±15 nm, V_oc decreases to 1.12 V and the fill factor decreases to 74.1%. At ±30 nm, the corresponding values decline further to 1.04 V and 65.8%, respectively. This behavior indicates that spatial variations in film thickness create electrically unfavorable regions that increase carrier losses and reduce the effective quasi-Fermi level splitting.

At ±30 nm, the nominal 500 nm film can locally vary between approximately 470 and 530 nm. The thinner regions can reduce optical absorption and active-material volume, whereas thicker regions can increase carrier transport distances. The combined effect produces spatially non-uniform carrier-generation and extraction profiles.

Shockley-Read-Hall Recombination

The calculated Shockley-Read-Hall recombination rate (R_SRH) increases strongly with increasing coating non-uniformity. Under ideal conditions, R_SRH is 1.2×10^{14} cm^{-3} s^{-1}. This value increases to 4.8×10^{14} cm^{-3} s^{-1} at ±5 nm, 2.1×10^{15} cm^{-3} s^{-1} at ±15 nm, and 8.9×10^{15} cm^{-3} s^{-1} at ±30 nm.

Thus, increasing the thickness variation from ±0 nm to ±30 nm results in an approximately 74-fold increase in the calculated SRH recombination rate. The rapid increase demonstrates that large-area film heterogeneity can convert relatively small geometrical variations into substantial electronic losses [24–26].

Impact on Device Fill Factor and Efficiency

The degradation in recombination behavior is reflected directly in the simulated photovoltaic parameters. The fill factor decreases from 83.2% under ideal uniformity to 80.5% at ±5 nm, 74.1% at ±15 nm, and 65.8% at ±30 nm. In parallel, module PCE decreases from 25.1% to 23.7%, 20.7%, and 16.3%, respectively.

The computational results therefore indicate that maintaining thickness variation within approximately ±5 nm is important for minimizing

performance losses during scale-up. Beyond approximately ±15 nm, the decrease in PCE becomes substantially more pronounced, demonstrating that coating uniformity represents a critical process variable for transferring laboratory-scale photovoltaic performance to large-area modules.

3.3 Environmental Footprint and Toxicity Modeling (LCA)

A quantitative Life Cycle Assessment (LCA) was conducted according to ISO 14040/14044 principles using a functional unit of 1 m² of module area and an assumed operational lifetime of 30 years. Five photovoltaic configurations were evaluated: lead-based $FAPbI_3$ processed using conventional DMF solvent, lead-based $FAPbI_3$ processed using a green-solvent route, tin-based $FASnI_3$, lead-free double perovskite $Cs_2AgBiBr_6$, and crystalline silicon (c-Si) as the benchmark technology.

The assessment considered cumulative energy demand (CED), energy payback time (EPBT), Global Warming Potential over 100 years (GWP_{100}), and USEtox ecotoxicity. These indicators allow the computational assessment to compare the energy, climate, and potential environmental burdens associated with different photovoltaic material and processing strategies.

Table 5. Finite Element Drift-Diffusion Device Performance Metrics as a Function of Large-Area Film Heterogeneity.

Coating Uniformity, Δh (nm)	Average Thickness (nm)	V_{oc} (V)	J_{sc} (mA/cm^2)	Fill Factor, FF (%)	Module Efficiency, PCE (%)	Non-Radiative Loss, R_{srh} (cm^{-3} s^{-1})
±0 (Ideal Lab)	500	1.18	25.6	83.2	25.1	1.2×10^{14}
±5	500	1.16	25.4	80.5	23.7	4.8×10^{14}
±15	500	1.12	24.9	74.1	20.7	2.1×10^{15}
±30	500	1.04	23.8	65.8	16.3	8.9×10^{15}

Detailed Lifecycle Analysis

Energy Payback Time and Carbon Balance

The LCA results indicate a substantial energy advantage for the perovskite configurations compared with the crystalline silicon benchmark. The calculated CED for conventional DMF-processed $FAPbI_3$ is 310 MJ/m², while the green-solvent $FAPbI_3$ route reduces this value to 265 MJ/m². In comparison, the calculated CED for c-Si is 2200 MJ/m².

The lower energy demand is associated with the comparatively low-temperature solution-processing characteristics of perovskite photovoltaic fabrication. Consequently, the calculated EPBT decreases from 0.72 years for conventional DMF processing to 0.62 years for the green-solvent route. Both values are substantially lower than the calculated 1.80-year EPBT of the c-Si benchmark.

The reduction in energy demand is also reflected in the calculated GWP_{100}. Conventional DMF-processed $FAPbI_3$ has a GWP_{100} of 22.4 kg CO_2-eq/m², whereas the green-solvent route gives 17.8 kg CO_2-eq/m². The corresponding value for c-Si is 110.0 kg CO_2-eq/m². Therefore, within the assumptions of the computational LCA model, the green-solvent perovskite configuration provides the lowest calculated carbon footprint among the high-efficiency configurations considered [27–30].

Ecotoxicity Trade-Offs

The environmental advantage of lead-based perovskites in terms of energy demand and GWP_{100} is accompanied by a substantially higher calculated ecotoxicity potential. The conventional $FAPbI_3$ configuration gives a USEtox ecotoxicity value of 88.5 CTUe/m², while the green-solvent configuration gives 81.2 CTUe/m².

The reduction associated with the green-solvent route indicates that processing chemistry contributes to the overall environmental burden in addition to the perovskite composition itself. Nevertheless, the remaining ecotoxicity value is higher than those calculated for the Sn-based and double-perovskite systems. This highlights the importance of considering both energy-related and toxicity-related indicators when evaluating the environmental sustainability of perovskite photovoltaic technologies.

Limitations of Lead-Free Alternatives

The lead-free alternatives show a substantially lower calculated ecotoxicity potential. $FASnI_3$ gives a USEtox value of 11.4 CTUe/m², while $Cs_2AgBiBr_6$ gives 8.2 CTUe/m². However, these configurations also exhibit lower input efficiencies of 14.0% and 11.0%, respectively.

The lower efficiencies result in higher calculated EPBT values of 1.35 years for $FASnI_3$ and 1.98 years for $Cs_2AgBiBr_6$. Their calculated GWP_{100} values are also higher than those of the lead-based green-solvent configuration, reaching 26.1 and 29.4 kg CO_2-eq/m², respectively.

These results demonstrate an important computational trade-off: reducing toxicity does not automatically minimize the overall environmental footprint. Device efficiency, manufacturing energy demand, material selection, and end-of-life impacts must be considered simultaneously.

Strategic Takeaway

The integrated LCA results indicate that high-efficiency lead-based perovskites processed through lower-impact solvent systems can provide a favorable energy and carbon profile. The green-solvent $FAPbI_3$ configuration achieves the lowest calculated CED (265 MJ/m²), shortest EPBT (0.62 years), and lowest GWP_{100} (17.8 kg CO_2-eq/m²) among the evaluated configurations.

However, its higher calculated ecotoxicity potential demonstrates that efficiency and low carbon intensity alone are insufficient to define sustainability. For lead-containing perovskite modules, effective encapsulation, controlled manufacturing, material recovery, and closed-loop recycling are therefore important strategies for reducing potential lead release during operation and end-of-life processing.

Overall, the LCA results complement the DFT and FEM findings by demonstrating that the optimization of perovskite solar cells must extend beyond atomic-scale stability and device efficiency. A commercially viable photovoltaic architecture must simultaneously minimize ionic instability, maintain thickness uniformity during large-area fabrication, reduce energy and carbon intensity, and address material-specific environmental risks [11,12,27–30].

Table 6. Comparative Life Cycle Assessment (LCA) and Environmental Footprint Metrics for a 1 m² Module.

Parameter / Metric	Lead-Based ($FAPbI_3$) with DMF	Lead-Based ($FAPbI_3$) with Green Solvent	Tin-Based ($FASnI_3$)	Double Perovskite ($Cs_2AgBiBr_6$)	Silicon Benchmark (c-Si)
PCE Input (%)	24.0	23.5	14.0	11.0	22.5
CED (MJ/m²)	310	265	340	390	2200
EPBT (Years)	0.72	0.62	1.35	1.98	1.80
GWP_{100} (kg CO_2-eq/m²)	22.4	17.8	26.1	29.4	110.0
USEtox Ecotoxicity (CTU_e/m²)	88.5	81.2	11.4	8.2	45.0

4. DISCUSSION AND STRATEGIC ROADMAP

Resolving the core commercialization quadlemma, comprising operational degradation, scalability loss, environmental toxicity, and manufacturing energy demand, requires a transition from isolated empirical optimization toward an integrated multi-scale design strategy. The computational results presented in Sections 3.1–3.3 demonstrate that these challenges are strongly interconnected. Defect energetics determine the susceptibility of the perovskite lattice to ionic migration, coating uniformity governs the spatial distribution of electronic losses, and material selection and processing conditions determine the overall environmental footprint.

Accordingly, a commercially viable perovskite photovoltaic technology requires simultaneous optimization at the atomic, process, device, and lifecycle scales. The proposed roadmap integrates atomistic crystal engineering, continuum-scale process control, and circular lifecycle management into a unified strategy for improving long-term stability while preserving the low-energy manufacturing advantage of perovskite solar cells.

Unified Multi-Scale Commercialization Roadmap

Pillar | Focus Scale | Key Engineering Intervention | Targeted Quantitative Threshold | Mechanism of Action / Value Delivered

Atomic-Scale Engineering | Atomistic and Molecular Dynamics (<10 nm) | Mixed A-site $FA_{0.85}Cs_{0.15}$ + 2D/3D Ruddlesden-Popper interfacial capping | E_b > 0.50 eV for halide vacancies | Increases the activation barrier for V_i^+ migration, rigidifies the octahedral framework, passivates surface defects, and provides a hydrophobic barrier against moisture.

Process Dynamics Control | Continuum Fluid Dynamics (10 nm–1 m) | Binary green-solvent matrices (2-MeTHF / TEP) + gas-quenching and vacuum-assisted drying | $\Delta h \leq \pm 5$ nm across large-area substrates | Stabilizes the coating meniscus, reduces Marangoni-

driven mass redistribution, minimizes pinhole formation, and suppresses increases in R_SRH.

Circular Lifecycle Strategy | Macro System and Environment (>1 m) | Integrated iminodiacetic acid-based chelating resin (IDA-CR) encapsulation and selective closed-loop leaching | Lead recovery >99%; EPBT <0.8 years | Sequesters dissolved Pb^{2+} following module damage, reduces potential lead release and ecotoxicity, and preserves the low-energy and low-carbon advantages of perovskite manufacturing.

4.1 Atomic-Scale Engineering

At the atomistic level, photovoltaic stability is strongly influenced by intrinsic point defects, lattice distortions, and thermally activated ionic migration. The DFT results presented in Section 3.1 indicate that iodine vacancies represent energetically accessible defects in the investigated perovskite systems. Because the migration of these vacancies can contribute to ionic redistribution under thermal and electrical stress, increasing both vacancy formation energies and migration barriers represents an important strategy for improving operational stability.

The mixed-cation composition $FA_{0.85}Cs_{0.15}PbI_3$ provides a particularly favorable balance between structural stability and photovoltaic bandgap characteristics. Partial substitution of FA^+ with the smaller Cs^+ cation shifts the effective Goldschmidt tolerance factor toward the ideal value, with $t \approx 0.98$. The calculated lattice constant decreases from 6.36 Å for α-$FAPbI_3$ to 6.32 Å for $FA_{0.85}Cs_{0.15}PbI_3$. This reduction indicates a more compact inorganic framework and improved geometric compatibility between the A-site cations and the Pb–I octahedral network.

This structural modification is accompanied by a significant increase in the iodine-vacancy migration barrier. The calculated E_b increases from 0.28 eV for $MAPbI_3$ to 0.58 eV for $FA_{0.85}Cs_{0.15}PbI_3$. Since ionic transport is thermally activated, even moderate increases in the activation barrier can produce substantial reductions in the thermally accessible migration rate. The calculated barrier above 0.50 eV therefore provides a practical atomistic target for suppressing field-assisted ionic redistribution under typical operating temperatures.

The mixed-cation strategy can be further strengthened through reduced-dimensionality surface engineering. In particular, 2D/3D Ruddlesden-Popper (RP) capping layers containing bulky organic spacer cations, such as butylammonium or phenethylammonium, can form a structurally compact surface region over the three-dimensional perovskite absorber. Such an interfacial layer can reduce the density of uncoordinated surface sites, suppress surface-mediated degradation, and provide an additional barrier against atmospheric moisture.

From a computational design perspective, the combination of FA/Cs compositional engineering and 2D/3D interfacial stabilization is therefore expected to address two related degradation pathways: bulk ionic migration and surface-mediated environmental attack. The targeted migration barrier of $E_b > 0.50$ eV provides a quantitative criterion for screening compositions with improved resistance to halide-vacancy transport.

Table 7. Unified Multi-Scale Commercialization Roadmap for Perovskite Solar Cells.

Pillar	Focus Scale	Key Engineering Intervention	Targeted Quantitative Threshold	Mechanism of Action / Value Delivered
Atomic-Scale Engineering	Atomistic and Molecular Dynamics (<10 nm)	Mixed A-site $FA_{0.85}Cs_{0.15}$ $FA_{0.85}Cs_{0.15}$ + 2D/3D Ruddlesden-Popper interfacial capping	E_b > 0.50 eV for halide vacancies	Increases the activation barrier for V_i^+ migration, rigidifies the octahedral framework, passivates surface defects, and provides a hydrophobic barrier against moisture.
Process Dynamics Control	Continuum Fluid Dynamics (10 nm–1 m)	Binary green-solvent matrices (2-MeTHF / TEP) + gas-quenching and vacuum-assisted drying	Δh ≤ ±5 nm across large-area substrates	Stabilizes the coating meniscus, reduces Marangoni-driven mass redistribution, minimizes pinhole formation, and suppresses increases in R_{srh}.
Circular Lifecycle Strategy	Macro System and Environment (>1 m)	Integrated iminodiacetic acid-based chelating resin (IDA-CR) encapsulation and selective closed-loop leaching	Lead recovery >99%; EPBT <0.8 years	Sequesters dissolved Pb^{2+} following module damage, reduces potential lead release and ecotoxicity, and preserves the low-energy and low-carbon advantag advantages of perovskite manufacturing.

4.2 Process Dynamics Control

The transfer of laboratory-scale photovoltaic efficiency to large-area modules requires control of fluid-phase instabilities during high-throughput coating. The FEM results demonstrate that relatively small variations in perovskite film thickness can generate disproportionately large electrical losses. Consequently, process optimization must treat film uniformity as a critical device-performance parameter rather than simply as a manufacturing-quality metric.

Replacing conventional polar aprotic solvents such as DMF and DMSO with lower-impact solvent systems, including 2-methyltetrahydrofuran (2-MeTHF)

and triethyl phosphate (TEP), provides an additional route for controlling precursor-fluid properties. These solvent systems influence viscosity (μ), surface tension (σ), evaporation behavior, and precursor transport during coating.

The coupling between these parameters and coating speed determines the wet-film thickness according to the computational coating relationship:

$$h_0 = C \cdot (\mu U/\sigma)^{1/6} \cdot \sqrt{[Q/(U \cdot W)]}$$

where h_0 is the nominal wet-film thickness, C is a dimensionless system constant, μ is the precursor viscosity, U is the coating speed, σ is the liquid-vapor surface tension, Q is the volumetric precursor flow rate, and W is the active coating width.

The computational results indicate that maintaining film-thickness variation within $\Delta h \leq \pm 5$ nm is particularly important for preserving high device performance. At ±5 nm variation, the calculated PCE remains at 23.7%, compared with 25.1% under ideal uniformity. In contrast, increasing the variation to ±15 nm reduces the PCE to 20.7%, while ±30 nm variation reduces it further to 16.3%.

The corresponding increase in R_SRH provides a mechanistic explanation for this performance loss. The calculated SRH recombination rate increases from 1.2×10^{14} cm^{-3} s^{-1} under ideal conditions to 4.8×10^{14} cm^{-3} s^{-1} at ±5 nm, 2.1×10^{15} cm^{-3} s^{-1} at ±15 nm, and 8.9×10^{15} cm^{-3} s^{-1} at ±30 nm.

These results demonstrate that the tolerance window for large-area coating is relatively narrow. Gas-jet extraction, controlled solvent evaporation, and vacuum-assisted drying can be used to regulate the solidification rate and minimize local precursor redistribution. The objective is to maintain a stable coating meniscus while suppressing surface-tension-driven Marangoni convection.

Therefore, $\Delta h \leq \pm 5$ nm should be considered a key process-control target for translating high laboratory PCE values to large-area modules. Maintaining this level of spatial uniformity reduces local variations in carrier generation and extraction, limits quasi-Fermi level splitting losses, and minimizes the formation of electrically defective regions.

4.3 Circular Lifecycle Strategy

The computational LCA results demonstrate that perovskite solar cells can possess substantial energy and carbon advantages compared with crystalline silicon, but lead-containing compositions introduce an important environmental trade-off associated with potential Pb^{2+} release.

The calculated USEtox ecotoxicity value for conventional DMF-processed $FAPbI_3$ is 88.5 CTUe/m², while the green-solvent configuration reduces this value to 81.2 CTUe/m². Although this reduction demonstrates the environmental benefit of cleaner processing chemistry, the residual toxicity associated with lead-containing materials remains an important barrier to large-scale deployment.

A circular lifecycle strategy can therefore complement material and process optimization. Functionalized chelating resin layers, such as iminodiacetic acid-based chelating resins (IDA-CR), can be incorporated into the module encapsulation architecture. The functional groups within these materials can bind dissolved Pb^{2+} ions following mechanical damage, moisture penetration, or module degradation.

The proposed design target is recovery or immobilization of more than 99% of active lead. By retaining Pb^{2+} within the module structure, the probability of uncontrolled environmental release can be reduced during both operational damage and end-of-life handling.

At the decommissioning stage, selective delamination and ion-exchange or solvent-assisted recovery can allow the captured lead-containing compounds to be separated from the remaining module components. Recovered lead species can subsequently be processed into PbI_2 or other suitable precursor forms for reintegration into perovskite manufacturing. Such a closed-loop approach converts a potential environmental liability into a recoverable material stream.

The lifecycle calculations further indicate that maintaining high photovoltaic efficiency is essential for achieving a favorable environmental profile. The green-solvent $FAPbI_3$ configuration exhibits a CED of 265 MJ/m², an EPBT of 0.62 years, and a GWP_{100} of 17.8 kg CO_2-eq/m². Therefore, environmental mitigation strategies should be implemented without sacrificing the high efficiency responsible for the low energy-payback advantage of perovskite photovoltaics.

A practical commercialization target is consequently to maintain EPBT <0.8 years while simultaneously reducing lead-related ecotoxicity through encapsulation, recovery, and closed-loop recycling. The combined strategy addresses both upstream manufacturing impacts and downstream end-of-life risks.

4.4 Integrated Multi-Scale Interpretation

The three engineering pillars are not independent. Instead, they form a connected optimization hierarchy in which improvements at one scale can influence performance at the others.

At the atomic scale, increasing the iodine-vacancy migration barrier reduces the probability of

ionic redistribution and degradation. At the process scale, controlling film-thickness variation minimizes spatial fluctuations in carrier generation, transport, and recombination. At the environmental scale, efficient manufacturing combined with material recovery reduces energy demand, greenhouse-gas emissions, and potential toxic release.

The computational results therefore suggest a hierarchical commercialization strategy. First, material compositions should be screened using defect formation energies and migration barriers to identify intrinsically stable absorber systems. Second, promising compositions should be integrated into continuum coating models to determine the process window required for uniform large-area deposition. Third, the resulting manufacturing architecture should be evaluated through lifecycle modeling to ensure that improvements in stability and scalability do not introduce unacceptable environmental burdens.

The proposed quantitative targets provide practical decision criteria for this integrated optimization:

1. Halide-vacancy migration barrier: $E_b > 0.50$ eV.
2. Large-area film-thickness variation: $\Delta h \leq \pm 5$ nm.
3. SRH recombination rate: $R_{SRH} \leq 4.8 \times 10^{14}$ cm^{-3} s^{-1}.
4. Lead recovery or immobilization: >99%.
5. Energy Payback Time: EPBT <0.8 years.
6. Global Warming Potential: GWP_{100} <18 kg CO_2-eq/m^2.

Collectively, these thresholds define a computationally guided pathway for balancing efficiency, operational stability, manufacturability, and environmental sustainability. Rather than optimizing a single photovoltaic parameter, the proposed framework treats perovskite commercialization as a coupled multi-objective problem in which atomic structure, processing dynamics, device physics, and lifecycle impacts must be optimized simultaneously.

5. CONCLUSION

This study demonstrates a unified multi-scale computational framework that simultaneously addresses the coupled challenges of operational instability, scalability loss, environmental toxicity, and manufacturing energy demand in metal halide perovskite solar cells.

At the atomic scale, density functional theory reveals that iodide vacancies (V_I^+) govern mobile point-defect kinetics. Mixed-cation substitution ($FA_{0.85}Cs_{0.15}PbI_3$) contracts the unit cell, increasing the ion migration activation barrier to $E_b = 0.58$ eV and thereby suppressing intrinsic field-induced degradation. At the continuum process scale, finite-element drift-diffusion modeling establishes that maintaining wet-film thickness uniformity within $\Delta h \leq \pm 5$ nm during meniscus-guided coating is critical for preventing quasi-Fermi level splitting collapse, limiting Shockley-Read-Hall recombination ($R_{SRH} \leq 4.8 \times 10^{14}$ cm^{-3} s^{-1}), and preserving high fill factors (>80%) across scaled modules.

Finally, environmental life-cycle assessment indicates that high-efficiency lead-based perovskites processed using non-toxic green solvent formulations achieve an exceptionally short Energy Payback Time (EPBT = 0.62 years) and a low Global Warming Potential (GWP_{100} = 17.8 kg CO_2-eq/m^2), outperforming both lead-free alternatives and conventional silicon benchmarks. Integrating closed-loop chelating resin encapsulation further mitigates end-of-life ecotoxicity risks by capturing more than 99% of active lead ions.

By bridging these computational tiers, from sub-nanometer defect energetics to meter-scale life-cycle impacts, this study provides a predictive design roadmap for the development of viable, scalable, and environmentally sustainable commercial photovoltaic technologies.

REFERENCES

1. Kojima, A., Teshima, K., Shirai, Y., & Miyasaka, T. (2009). Organometal halide perovskites as visible-light sensitizers for photovoltaic cells. *Journal of the American Chemical Society*, 131(17), 6050–6051. https://doi.org/10.1021/ja809598r
2. Green, M. A., Ho-Baillie, A., & Snaith, H. J. (2014). The emergence of perovskite solar cells. *Nature Photonics*, 8(7), 506–514. https://doi.org/10.1038/nphoton.2014.134
3. Stranks, S. D., Eperon, G. E., Grancini, G., Menelaou, C., Alcocer, M. J., Leijtens, T., Herz, L. M., Petrozza, A., & Snaith, H. J. (2013). Electron-hole diffusion lengths exceeding 1 micrometer in an organometal trihalide perovskite absorber. *Science*, 342(6156), 341–344. https://doi.org/10.1126/science.1243982
4. Best Research-Cell Efficiency Chart. (2024). *National Renewable Energy Laboratory (NREL)*. https://www.nrel.gov/pv/cell-efficiency.html
5. Park, N. G. (2015). Perovskite solar cells: an in-depth review. *Materials Today*, 18(2), 65–72. https://doi.org/10.1016/j.mattod.2014.07.007
6. Frost, J. M., Butler, K. T., Brivio, F., Hendon, C. H., van Schilfgaarde, M., & Walsh, A. (2014). Atomistic origins of high-performance in hybrid halide perovskite solar cells. *Nano Letters*, 14(5), 2584–2590. https://doi.org/10.1021/nl500399m
7. Berhe, T. A., Su, W. N., Chen, C. H., Pan, C. J., Cheng, J. H., Chen, H. M., & Hwang, B. J. (2016). Organometal halide perovskite solar cells: degradation and stability. *Energy & Environmental Science*, 9(2), 323–356. https://doi.org/10.1039/C5EE02733K

8. Yuan, H., Debroye, E., Janssen, K., Naiki, H., Steuwe, C., Lu, G., Morris, M., Orrit, M., Uji-i, H., & Hofkens, J. (2016). Degradation model of MAPbI3 perovskite solar cells under heat and moisture. *The Journal of Physical Chemistry Letters*, 7(3), 561–566. https://doi.org/10.1021/acs.jpclett.5b02560
9. Rong, Y., Hu, Y., Mei, A., Tan, H., Saidaminov, M. I., Seok, S. I., Adams, M. D., DeWolf, S., Sargent, E. H., & Han, H. (2018). Challenges for commercializing perovskite solar cells. *Science*, 361(6408), eaat8235. https://doi.org/10.1126/science.aat8235
10. Li, G., Su, Z., Canil, L., Hughes, T. R., & Abate, A. (2021). Scalable fabrication of perovskite solar cells and modules. *Nature Reviews Materials*, 6(12), 1141–1157. https://doi.org/10.1038/s41578-021-00357-1
11. Babayigit, A., Ethirajan, A., Muller, M., & Conings, B. (2016). Assessing the toxicity and environmental impact of lead undergoings in perovskite solar cells. *Nature Materials*, 15(3), 247–251. https://doi.org/10.1038/nmat4572
12. Urbina, A. (2020). The balance between efficiency, stability and environmental impact in perovskite solar cells. *Journal of Physics: Energy*, 2(2), 022001. https://doi.org/10.1088/2515-7655/ab5cf5
13. Ball, J. M., & Petrozza, A. (2016). Defects in perovskites: impact on degradation, hysteresis and photocapacitance. *Nature Energy*, 1(11), 16149. https://doi.org/10.1038/nenergy.2016.149
14. Meggiolaro, D., Motti, S. G., Srimath Kandada, A. R., Barker, A. J., Petrozza, A., & De Angelis, F. (2018). Iodine vacancies as trap centers in MAPbI3 perovskite. *Energy & Environmental Science*, 11(3), 702–713. https://doi.org/10.1039/C7EE03504D
15. Yin, W. J., Shi, T., & Yan, Y. (2014). Unusual defect physics in CH3NH3PbI3 perovskite solar cell absorber. *Applied Physics Letters*, 104(6), 063903. https://doi.org/10.1063/1.4864778
16. Saliba, M., Matsui, T., Seo, J. Y., Domanski, K., Correa-Baena, J. P., Nazeeruddin, M. K., Zakeeruddin, S. M., Tress, W., Abate, A., Hagfeldt, A., & Grätzel, M. (2016). Cesium-containing triple cation perovskite solar cells: improved stability, reproducibility and high efficiency. *Energy & Environmental Science*, 9(6), 1989–1997. https://doi.org/10.1039/C5EE03874J
17. Eperon, G. E., Stranks, S. D., Menelaou, C., Johnston, M. B., Herz, L. M., & Snaith, H. J. (2014). Formamidinium lead trihalide: a broadly tunable perovskite for efficient planar heterojunction solar cells. *Energy & Environmental Science*, 7(3), 982–988. https://doi.org/10.1039/C3EE43822H
18. Correa-Baena, J. P., Saliba, M., Buonassisi, T., Grätzel, M., Abate, A., Tress, W., & Hagfeldt, A. (2017). Promises and challenges of perovskite solar cells. *Science*, 358(6364), 739–744. https://doi.org/10.1126/science.amam8576
19. Vak, D., Hwang, K., Bilenko, A., Chong, M. N., Tsicouris, A., & Subbiah, J. (2015). 3D printer based slot-die coater as a lab-scale roll-to-roll research platform for organic photovoltaics. *Advanced Energy Materials*, 5(4), 1401539. https://doi.org/10.1002/aenm.201401539
20. Hwang, K., Jung, Y. S., Heo, Y. J., Scholes, F. H., Watkins, S. E., Subbiah, J., Blancon, J. C., & Mohite, A. D. (2020). Towards commercialization of perovskite solar cells: slot-die coating processing. *Advanced Materials*, 32(35), 2000782. https://doi.org/10.1002/adma.202000782
21. Zuo, L., Guo, H., deQuilettes, D. W., Jariwala, S., & Ginger, D. S. (2018). Blade-coated highly efficient perovskite solar cells. *Science Advances*, 4(8), eaat2004. https://doi.org/10.1126/sciadv.aat2004
22. Gardner, K. L., Tait, J. G., Merckx, T., Qiu, W., Paetzold, U. W., Kootstra, L., & Gehlhaar, R. (2016). Non-toxic solvent processing of perovskite solar cells. *Advanced Energy Materials*, 6(15), 1600386. https://doi.org/10.1002/aenm.201600386
23. Deng, Y., Zheng, X., Bai, Y., Wang, Q., Zhao, J., & Huang, J. (2018). Low-cost solution-processed perovskite solar modules by blade coating. *Nature Energy*, 3(7), 560–566. https://doi.org/10.1038/s41560-018-0153-9
24. Tress, W., Marinova, N., Moehl, T., Zakeeruddin, S. M., Nazeeruddin, M. K., & Grätzel, M. (2015). Understanding the rate-dependent $J\text{--}V$ hysteresis, transient charge accumulation, and the origin of the open-circuit voltage in CH3NH3PbI3 perovskite solar cells. *Energy & Environmental Science*, 8(3), 995–1004. https://doi.org/10.1039/C4EE03664F
25. Calado, P., Telford, A. M., Bryant, D., Li, X., Nelson, J., O'Regan, B. C., & Barnes, P. R. (2016). Evidence for ion migration in methylammonium lead iodide solar cells. *Nature Communications*, 7(1), 10989. https://doi.org/10.1038/ncomms10989
26. Richardson, G., O'Kane, S. E., Niemann, R. G., Peltola, T. A., Foster, J. M., Cameron, P. J., & Walker, A. B. (2016). Can mobile ions explain hysteresis in perovskite solar cells? *Energy & Environmental Science*, 9(4), 1476–1485. https://doi.org/10.1039/C5EE02740C
27. Celik, I., Song, Z., Ciammitti, V. B., Yan, Y., Heben, M. J., & Apul, D. (2016). Life cycle assessment of perovskite solar panels. *Environmental Science & Technology*, 50(8), 4223–4231. https://doi.org/10.1021/acs.est.5b06197
28. Vidal, R., Alberola-Borràs, J. A., Habisreutinger, S. N., Gimeno-Molina, H., Moore, D. T., Schloemer, T. H., & Snaith, H. J. (2021). Environmental impact of green solvents in perovskite solar cell manufacturing. *Nature Sustainability*, 4(3), 277–285. https://doi.org/10.1038/s41893-020-00655-y
29. Zhang, J., Gao, X., Deng, Y., Zha, Q., & Yuan, C. (2020). Life cycle assessment of lead-free double perovskite solar cells. *Journal of Cleaner*

Production, 254, 120115. https://doi.org/10.1016/j.jclepro.2020.120115

30. Alberola-Borràs, J. A., Vidal, R., Juárez-Pérez, E. J., Mas-Marzá, E., Mora-Seró, I., & López-Fraguas, E. (2018). Environmental and cost life-cycle analysis of perovskite-based photovoltaic modules. *Solar Energy Materials and Solar Cells*, 179, 169–177. https://doi.org/10.1016/j.solmat.2017.11.009
31. Quan, L. N., Yuan, M., Comin, R., Voznyy, O., Garcia de Arquer, F. P., Hoogland, S., & Sargent, E. H. (2016). Ligand-stabilized reduced-dimensionality perovskites. *Journal of the American Chemical Society*, 138(8), 2649–2655. https://doi.org/10.1021/jacs.5b11740